J. Fluid Mech. (1994), *vol.* 259, *pp.* 167–189

The diode-array velocimeter

By WILLIAM J. DEVENPORT AND EDWARD J. SMITH

Department of Aerospace and Ocean Engineering, Virginia Polytechnic Institute and State University, Blacksburg, VA 24061, USA

(Received 4 March 1993 and in revised form 16 July 1993)

Diode-array velocimetry is an optical technique for measuring turbulent flows. It involves timing the passage of seed particles through a small section of a light beam by imaging the light they scatter onto one or more photodiode arrays. The arrays have a few carefully shaped elements, the shapes and positions of which are used to control the measurement-volume geometry and thus select the measurement made. Measurement volumes sensitive to velocity, position and acceleration may be designed. Measurements in highly turbulent and reversing flows are possible.

A diode-array velocimeter (DAV) for one-component velocity measurements has been developed to demonstrate this concept. This uses a single laser beam to illuminate particles and a photodiode array with two rectangular elements to sense their motion. The sensitivity of this DAV to electrical noise in the photodiode circuitry decreases with reduction in measurement-volume size. The angle response is closely cosinusoidal to about 60°. Changes to the photodiode-array design could substantially increase this limit.

Measurements of mean velocity, normal turbulence stress and velocity skewness made with this DAV in two attached boundary-layer flows compare well with hot-wire measurements. Useful DAV measurements were made as close as 0.2 mm from the wall. DAV measurements made in a separated flow formed downstream of a fence are also presented. These show all the expected features of the separated shear layer and recirculation including the sub-boundary layer formed beneath the backflow. Histograms measured in the reversing part of this flow show a hole near zero velocity that is a consequence of the imperfections in the DAV angle response and limitations on the maximum transit time. These are not fundamental problems, however, and the hole could be minimized or eliminated by using a different photodiode array design and/or measurement strategy.

1. Introduction

The diode-array velocimeter (DAV) is a device for measuring turbulent flows. The simplest possible optical layout of a DAV is shown in figure 1. A single light beam is directed into a flow. Particles in the flow, either naturally occurring or artificially introduced, scatter light as they pass through the beam. Scattered light from a small section of the beam is collected by a lens and focused onto a photodiode array with a few carefully shaped elements. As particles pass through the beam their images pass across the array elements. Measurements are made by timing this passage.

The measurement volume implied by this optical arrangement is the intersection of the light beam and the projection of the photodiode-array elements back through the receiving lens. The form of the measurement volume depends on the number, shape and position of the elements, the beam size and the receiving lens orientation and magnification. It is chosen to make the deduction of flow properties from the measured

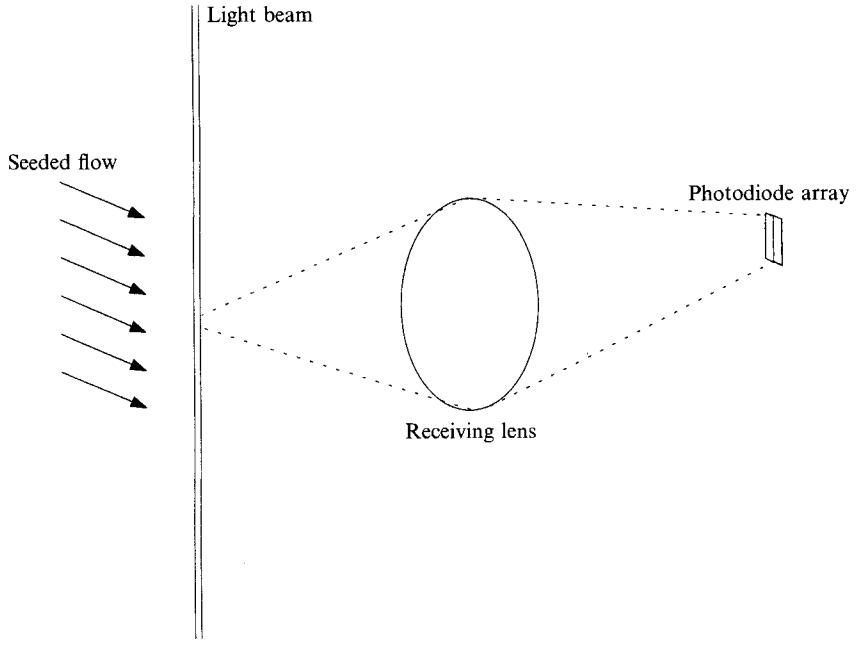

FIGURE 1. Simplest possible optical layout for a DAV.

transit times simple and accurate. Measurement volumes sensitive to particle velocity, position and acceleration may be designed. By using more than one photodiode array and/or more than one receiving lens, simultaneous two- and three-component measurements should also be possible.

The idea of using a single beam or an array of detectors in an anemometer is not new. For example, Boutier & Lefevre (1988) used an array of optical fibres and a series of photo-multiplier tubes to detect velocities with a single laser beam. Hirleman *et al.* (1984) used only one detector and one beam, the transit time of particles through the laser beam being measured. Detector arrays have been used in some laser-two-focus systems (see for example Ohmura, Hishada & Maeda 1992). The drawback of all these types of schemes has been their poor accuracy when compared to laser-Doppler anemometry.

What is new about the DAV concept is its use of photodiode-array geometry; both the shapes of the elements and their positions are exploited to select the form of the measurement volume and thus the measurement made. Silicon photodiode arrays can be made in almost any shape and pattern and are therefore well suited to this application.

In velocity measurements the DAV concept has, at least in principle, some significant advantages over competing techniques. Compared to laser-Doppler anemometry the DAV is simple, requiring only one (not necessarily coherent or monochromatic) illuminating beam regardless of the number of components to be measured. In addition the signals it produces (electrical pulses indicating the passage of a particle image over a photodiode element) are easier and cheaper to process than frequency-modulated bursts. Optical simplicity is also an advantage in comparison to laser-two-focus anemometry, as are accuracy and the ability to make velocity measurements regardless of turbulence level and flow reversals.

This paper describes the design and construction of a DAV for one-component velocity measurements. This system is analysed and its performance in attached and

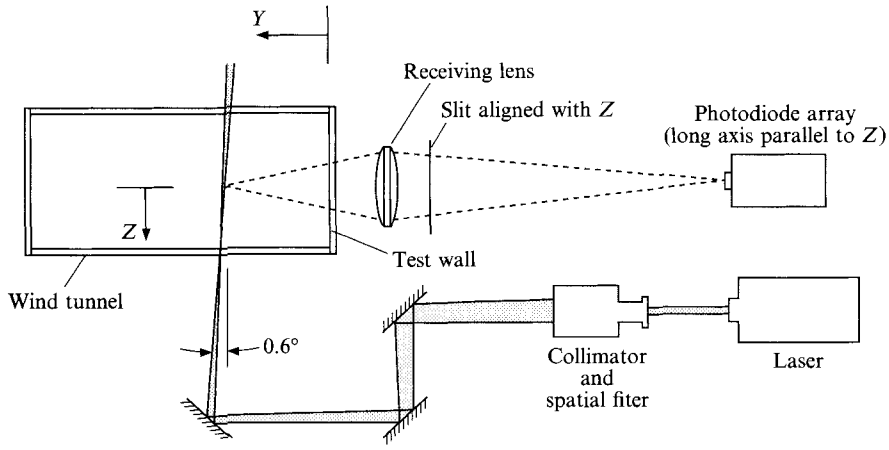

FIGURE 2. Schematic showing the optical system of the one-component DAV and the wind-tunnel cross-section.

separated flows examined. The primary objective of this work was to demonstrate the viability of the DAV concept.

2. Design of the one-component DAV

2.1. *Optical system*

The basic form of the optical system is illustrated in figure 1. A more detailed schematic is shown in figure 2. The essential components are a collimated light source, a lens and a photodiode array. A Spectra Physics model 164 argon-ion laser was used as the light source since this was already available. Operated at a wavelength of 514.5 nm, it produced a 1 W beam of Gaussian intensity distribution. An Oriel Corporation 50 mm diameter, 100 mm focal length achromat was used as the receiving lens based on its low cost, and ability to collect a reasonable solid angle of scattered light and form a high-quality image. The photodiode array chosen was the Silicon Detector Corporation SD160, illustrated in figure 3. It consists of two rectangular PIN photodiode elements, each 4.57×0.51 mm, placed side by side and separated by a distance of 0.02 mm. As will be discussed later this geometry, while adequate, is not the best possible for a one-component DAV. The SD160 was chosen because it was the most suitable device already in commercial production.†

In addition to these essential components, an Oriel model 15261 collimator and 10 μm spatial filter were used to vary the diameter of the laser beam and ensure its Gaussian intensity distribution in the measurement volume. A 12.7 mm wide slit, placed adjacent to the receiving lens was used to improve depth of focus. Several front-surface mirrors were also used to position the beam. All optical components were mounted on an aluminium table built on a traversible milling machine base.

With its components fixed, design of the optical system involves four variables: (i) the laser beam diameter, (ii) the angle of the receiving lens axis to the laser beam (the receiver angle), (iii) the orientation of the detector array, and (iv) the distance of the receiving lens from the beam (i.e. the optical magnification M of scattering particle images). The beam diameter (0.4 mm at the $1/e^2$ points) and optical magnification ($\times 10$) were chosen as a consequence of design constraints described in the following

† Building a PIN photodiode array to a new design initially costs between \$10000 and \$20000. Subsequent devices of the same design, however, typically cost \$50 to \$100 each.

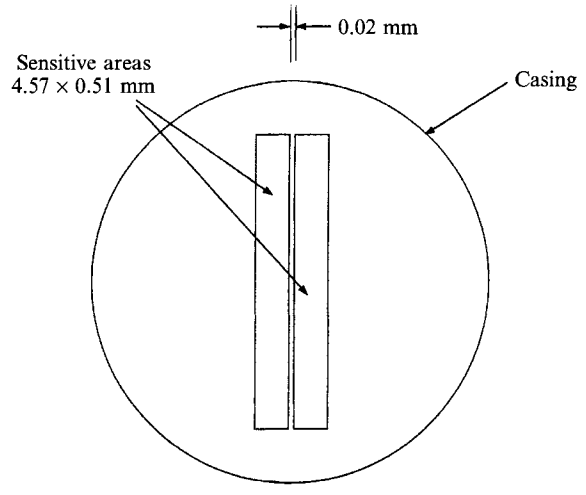

FIGURE 3. The Silicon Detector Corporation SD160 photodiode array.

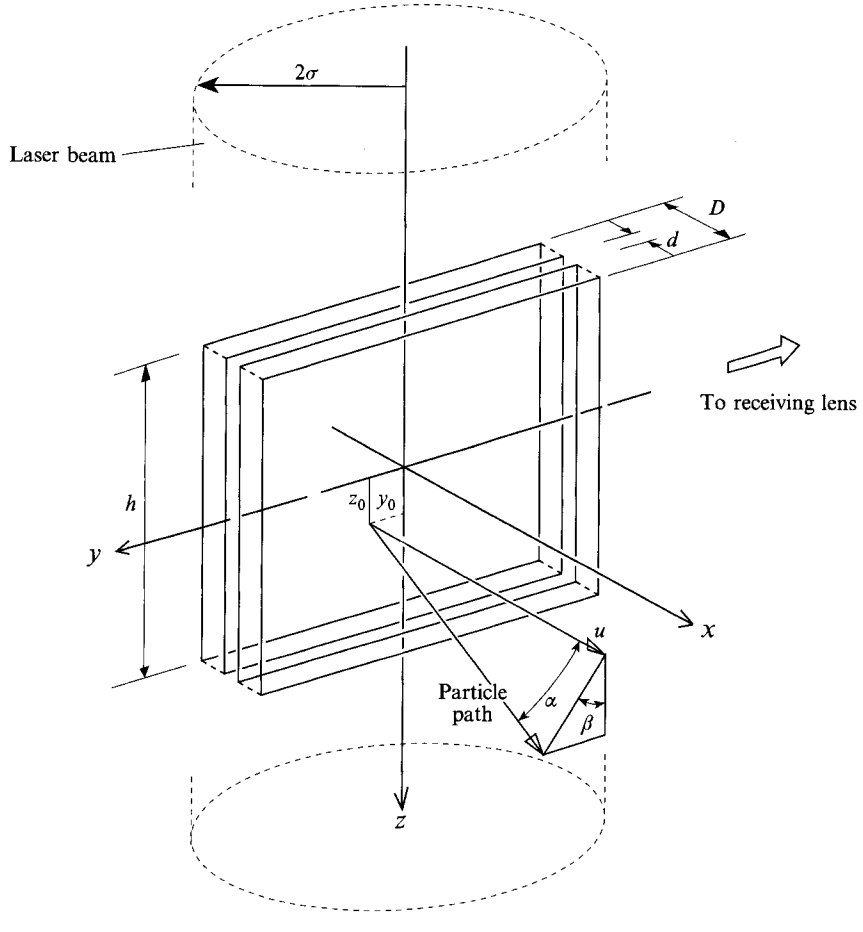

FIGURE 4. Measurement volume of the one-component DAV.

sections. To give the simplest possible measurement-volume shape, the receiver angle was fixed at 90° and the detector array was oriented with its face normal to the receiving-lens axis and with the long edges of its rectangular elements parallel to the laser beam. The measurement volume thus formed consists of two parallel 'plates' (figure 4), suitable for measurements of the velocity component u. Its length ($h = 0.457$ mm), overall width ($D = 0.104$ mm) and separation of its two halves ($d = 0.002$ mm) are equal to the corresponding dimensions of the photodiode array divided by the magnification of the receiving lens. Its depth is the diameter of the laser beam.

2.2. *Obtaining signals from the photodiode array*

The elements of the photodiode array were operated independently, each with a circuit of the type shown in figure 5. This circuit places a bias voltage across the photodiode element, causing it to convert the light power it receives into a proportional current. This current is then converted to a voltage using a transimpedance amplifier with a feedback resistance (and therefore current to voltage gain) of $7 \times 10^6\ \Omega$.

The dynamic characteristics of these circuits were determined by simultaneously exciting both photodiode elements with a green-light-emitting diode of flat frequency response (Hewlett Packard HPMP-3507). The results, plotted in figure 6, show the circuits to be closely matched, with 3 dB points at around 140 kHz. The frequency response of this type of circuit is limited by stray capacitance across the resistor, this acting to reduce the feedback impedance at higher frequencies. The r.m.s. output noise level was about 1.5 mV for both circuits.

Figure 7 shows typical DAV signals output from the amplifiers over a range of flow conditions for 2.1 μm seeding particles. Note that the origins of the voltage scales in this figure are arbitrary. These signals are formed as follows. A particle, moving at constant speed through the Gaussian laser beam produces an image in the receiving lens whose light power varies as a Gaussian with time. As the image crosses the photodiode array each element detects a portion of this Gaussian. The detection and amplification of these signals filters them and adds noise. Note that, since the particle may enter the measurement volume at any angle and not pass through the beam centre the photodiode elements may see unsymmetrical portions of the Gaussian (see for example figure 7*c*, *e*). The amplitude of these voltage signals (typically 100 mV) combined with the sensitivity of the photodiode elements (about $0.2\ \mathrm{A\ W^{-1}}$ at 514.5 nm) implies a light power in the particle images of the order of tens of nW, consistent with the results of Mie scattering calculations.

2.3. *Timing*

To determine the magnitude and sign of the velocity component u (figure 4), the transit time of particles between the centres of the measurement volume 'plates' and the order in which the 'plates' are crossed must be extracted froim the amplifier output signals. A simple way of accomplishing both these measurements is to cross-correlate the signals – the magnitude and sense of the time delay of peak correlation coefficient giving the transit time and flow direction respectively.

As will be shown in the following sections this scheme has some desirable characteristics. However, it is only one of many possible methods and ignores some possibly useful information, e.g. the magnitude of the signal peaks, which can be related to the particle position. Another simple scheme that we are studying involves connecting the amplifier outputs to two Schmitt triggers designed to fire when the voltage rises significantly above the noise level. A digital clock is used to determine the transit time by timing the interval between the firing of the triggers. A logic circuit

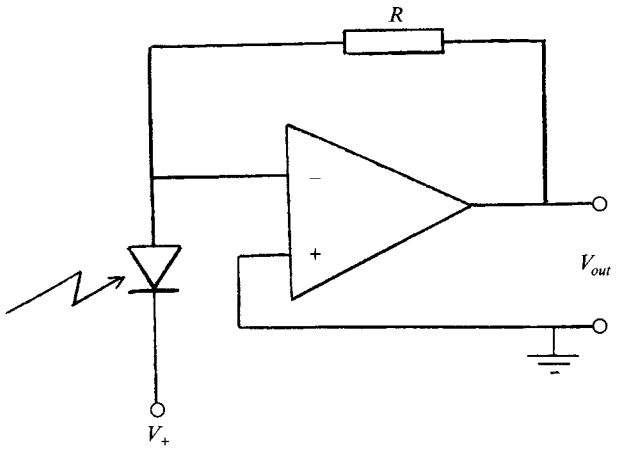

FIGURE 5. Circuit used to amplify current signals produced by photodiode element. $R = 7 \times 10^6\ \Omega$. $V_+ = 15$ V. Amplifier is a Burr–Brown OPA 627.

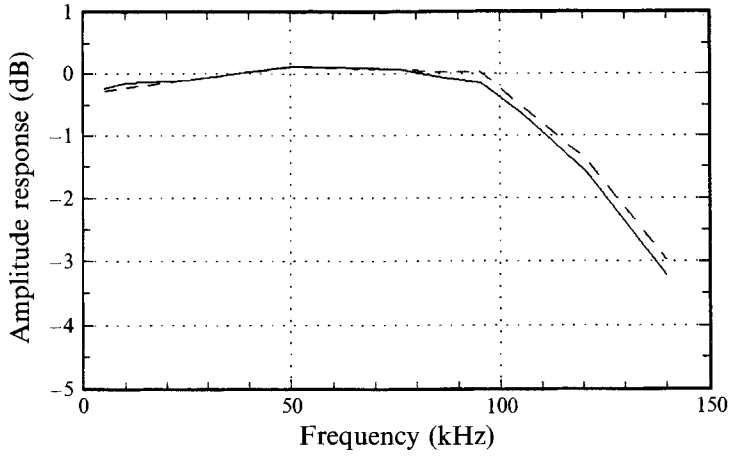

FIGURE 6. Frequency response curves for the photodiode elements and their amplifiers: solid line, channel 1 (upstream); dashed line, channel 2 (downstream).

detects which trigger was fired first and thus the flow direction. A discrimination circuit ensures that only signals with amplitudes substantially greater than the trigger level are measured. This method, discussed in more detail by Devenport & Smith (1993), has the advantage that it can be performed entirely using a simple purpose-built electronic circuit that could easily be miniaturized. Its primary disadvantage, compared to cross-correlation, is a greater sensitivity to noise.

3. Theoretical analyses

3.1. *Influence of noise in determining velocity*

The relationship between the transit time t determined from the DAV signals and the velocity u inferred from it is ideally

$$u = A/t, \tag{1}$$

where A is the distance between the centres of the measurement volume plates $\frac{1}{2}(D+d)$,

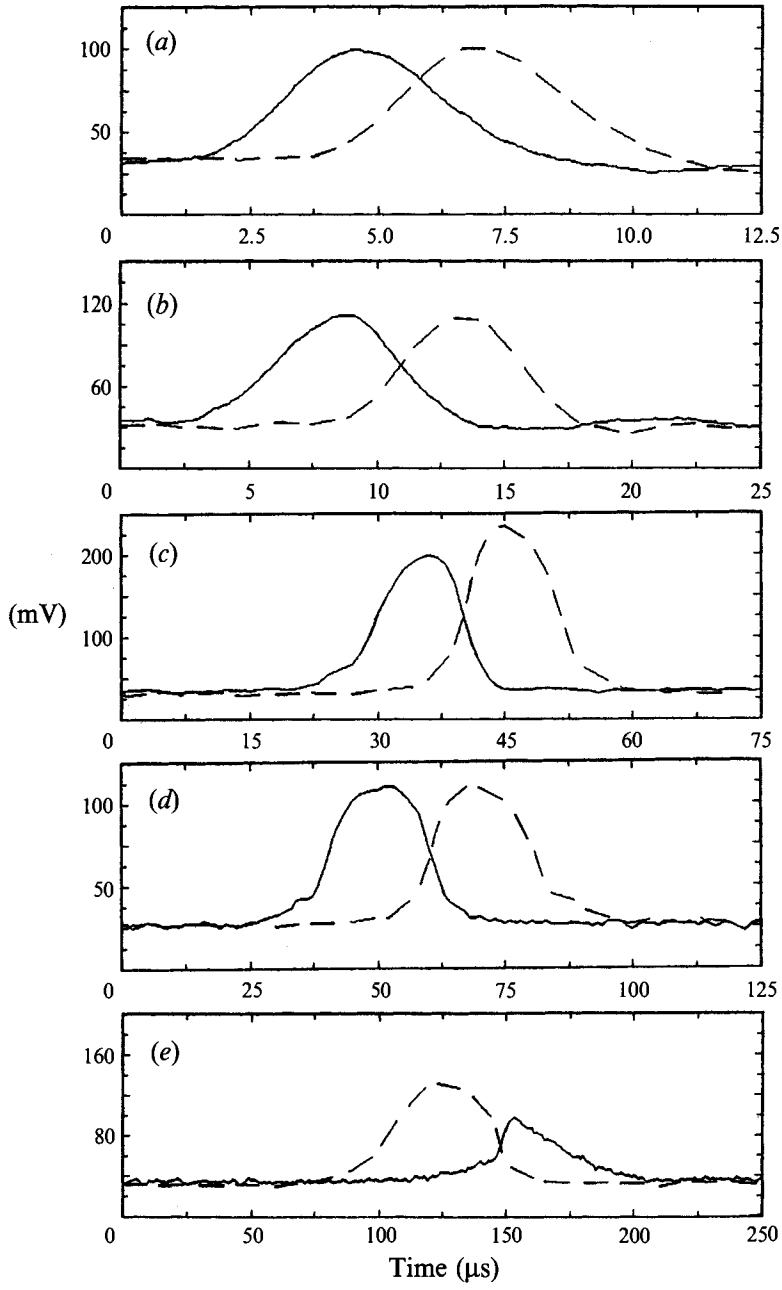

FIGURE 7. Typical DAV output signals: solid line, channel 1 (upstream); dashed line, channel 2 (downstream). (*a*) 20.6 m s^{-1}, (*b*) 9.9 m s^{-1}, (*c*) 4.5 m s^{-1}, (*d*) 2.4 m s^{-1}, (*e*) -1.4 m s^{-1}.

see figure 4. This measured transit time may be thought of as having contributions from the actual transit time and electrical noise t'_n. Over a sequence of many samples the actual transit time may be thought of as being made up of a mean T and a fluctuation t'_t associated with unsteadiness in the flow. We may therefore write

$$u = \frac{A}{T + t'_t + t'_n}. \tag{2}$$

As indicated t'_n would not be expected to have a mean value. It is simple to show that, to a first-order approximation assuming $t'_n \ll T$ and $t' \ll T$, equation (2) leads to the expressions

$$U \approx A/T, \tag{3}$$

$$\frac{\overline{u'^2}}{U^2} \approx \frac{\overline{t'^2_t} + \overline{t'^2_n}}{T^2} \approx (\overline{t'^2_t} + \overline{t'^2_n})\frac{U^2}{A^2}, \tag{4}$$

where U and u' represent the measured mean velocity and velocity fluctuation respectively. So, assuming constant $\overline{t'^2_n}$, the influence of electrical noise on normalized turbulence stress measurements should increase as the square of the mean velocity. Obviously, minimizing electrical noise is important if accurate turbulence measurements are desired.

Whether the transit time is being determined using a cross-correlation or trigger scheme we would expect the r.m.s. of t'_n to rise if the electrical signal-to-noise ratio S (peak signal voltage divided by r.m.s. voltage noise level) were decreased. We would also expect it to rise if the amplifier cutoff frequency ω_c were reduced since this would lead to greater filtering of the signals, blurring their definition in time. As shown in the Appendix, it follows that

$$\frac{(\overline{t'^2_n})^{\frac{1}{2}}}{T} \sim \frac{1}{S\omega_c T}. \tag{5}$$

Since voltage noise in the DAV outputs is independent of signal, S depends only on the peak signal magnitude. This, in turn, will vary linearly with the total light power received in a particle image, which is proportional to the intensity of the laser beam multiplied by the solid angle over which the receiving lens collects light. Using f_1 and l to denote the distance from the measurement volume to the receiving lens and the lens diameter respectively, we have

$$S \sim \frac{P}{\sigma^2}\frac{l^2}{f_1^2} = \frac{P}{\sigma^2 f^{\#2}}\left(\frac{M}{M+1}\right)^2, \tag{6}$$

where P is the total laser beam power, σ is its r.m.s. width, $f^{\#}$ is the f-number of the receiving lens and M is the image magnification it produces. Now, for the measurement-volume geometry to remain constant then we must have

$$\sigma \sim 1/M \tag{7}$$

and so

$$S \sim \frac{P}{f^{\#2}}\frac{M^4}{(M+1)^2}. \tag{8}$$

Substituting back into (5) gives

$$\frac{(\overline{t'^2_n})^{\frac{1}{2}}}{T} \sim \frac{f^{\#2}(1+M)^2}{PM^4}\frac{1}{\omega_c T}. \tag{9}$$

For a given flow velocity, T is inversely proportional to M, since optical magnification amplifies the speed of the particle image as well as its size and so, finally, we have

$$\frac{(\overline{t'^2_n})^{\frac{1}{2}}}{T} \sim \left(\frac{f^{\#2}}{P\omega_c}\right)\left(\frac{(M+1)^2}{M^3}\right). \tag{10}$$

The first term on the right-hand side of (10) is fixed by the choice of optical and electrical components. To minimize the influence of noise on velocity measurements

the receiving-lens magnification should therefore be maximized and the laser-beam diameter correspondingly reduced. These measures have the added benefits of minimizing the measurement-volume size and maximizing signal-to-noise ratio (making the presence of a signal much easier to detect).

For the present DAV, M was set at 10, this being the maximum that could be achieved with the available optical table. In fixing the aperture, and thus the $f^{\#}$ of the receiving lens, depth of focus was found to be an important consideration. If particle images are out of focus this smooths the rising and falling edges of the output signals. The net effect is similar to that of a decrease in ω_c. Focusing of particle images in the direction normal to the long axis of the photodiode array was improved using the 12.7 mm wide slit shown in figure 2.

3.2. *Linearity and angle response*

Linearity and angle response were studied by simulating signals produced by the DAV over a range of conditions. Consider the measurement volume of figure 4. Taking the laser beam as Gaussian, its normalized intensity distribution I can be written as

$$I(x,y) = \exp\left(-\frac{x^2+y^2}{2\sigma^2}\right), \tag{11}$$

where σ is the r.m.s. beam width (one quarter of its $1/e^2$ diameter) and the coordinate system (x,y,z) is centred in the measurement volume with the z-axis parallel to the beam (figure 4).

Consider a particle with a velocity (u,v,w) moving along a trajectory that crosses the measurement-volume centreplane at the location $(0,y_0,z_0)$. The particle will experience a light intensity equal to

$$\exp\left(-\frac{x^2+((y-y_0)+y_0)^2}{2\sigma^2}\right), \tag{12}$$

which may be rewritten in terms of time t as

$$\exp\left(-\frac{(ut)^2+(vt+y_0)^2}{2\sigma^2}\right). \tag{13}$$

Assuming the light power scattered by the particle is proportional to that incident upon it and that the diameter of the particle and its image are negligible, this expression may also be used to represent the normalized light power received or current signals produced by the photodiode elements. All that is needed is to state the limits of the signal for each element. These are

for element 1: $\quad -\frac{1}{2}D < ut < -\frac{1}{2}d, \quad -\frac{1}{2}h < wt+z_0 < \frac{1}{2}h,$

for element 2: $\quad \frac{1}{2}d < ut < \frac{1}{2}D, \quad -\frac{1}{2}h < wt+z_0 < \frac{1}{2}h,$

where d, D and h are the dimensions of the measurement volume defined in figure 4. Introducing q to denote the magnitude of the velocity vector $(u^2+v^2+w^2)^{\frac{1}{2}}$, angles α and β to denote its direction (see figure 4) and the non-dimensional variable $t^* = qt/\sigma$, these current signals may be rewritten as

$$\mathrm{i}(t^*) = \exp\left(-\tfrac{1}{2}(t^*\cos\alpha)^2 - \tfrac{1}{2}(t^*\sin\alpha\sin\beta + y_0/\sigma)^2\right); \tag{14}$$

for element 1:

$$-\tfrac{1}{2}D/\sigma < t^*\cos\alpha < -\tfrac{1}{2}d/\sigma, \quad -\tfrac{1}{2}h/\sigma < t^*\sin\alpha\cos\beta + z_0/\sigma < \tfrac{1}{2}h/\sigma,$$

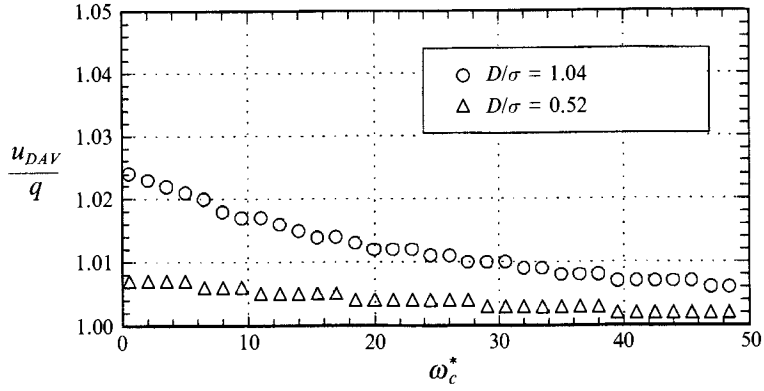

FIGURE 8. Velocity inferred from simulated DAV signals over actual velocity as a function of ω_c^* for zero pitch and yaw. For the present system $D/\sigma = 1.04$.

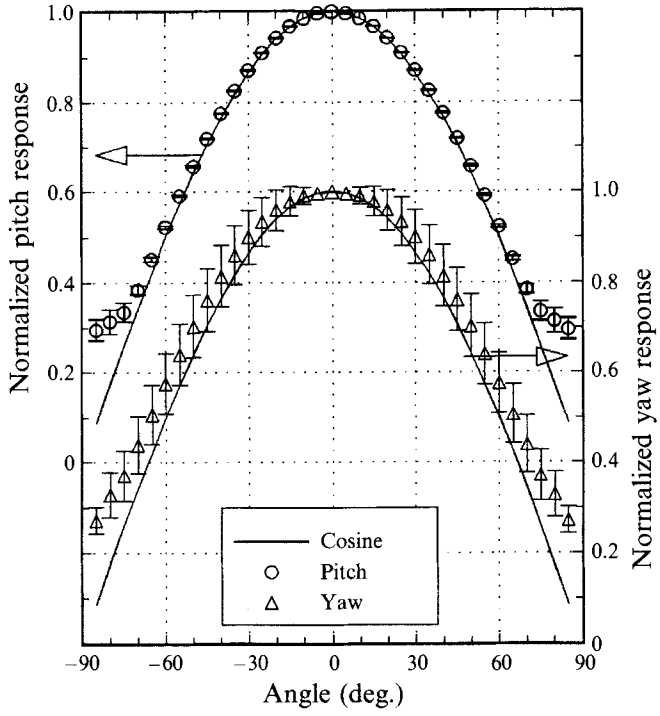

FIGURE 9. DAV angle response normalized on velocity at zero pitch and yaw, $\omega_c^* = 5.65$, no conditions on peak correlation coefficient. Points show average over measurement volume, error bars show r.m.s. variation.

for element 2:

$$\tfrac{1}{2}d/\sigma < t^* \cos\alpha < \tfrac{1}{2}D/\sigma, \quad -\tfrac{1}{2}h/\sigma < t^* \sin\alpha \cos\beta + z_0/\sigma < \tfrac{1}{2}h/\sigma.$$

The current-to-voltage converters amplify and filter these signals. Their output is given by

$$v(t) = \mathrm{i}(t) * h(\omega_c t), \tag{15}$$

where $h(\omega_c t)$ is the amplifier impulse response, ω_c is the angular cutoff frequency of that response and the asterisk denotes convolution. Non-dimensionalizing gives

$$v(t^*) = \mathrm{i}(t^*) * h(\omega_c^* t^*), \tag{16}$$

where $\omega_c^* = \omega_c \sigma/q$.

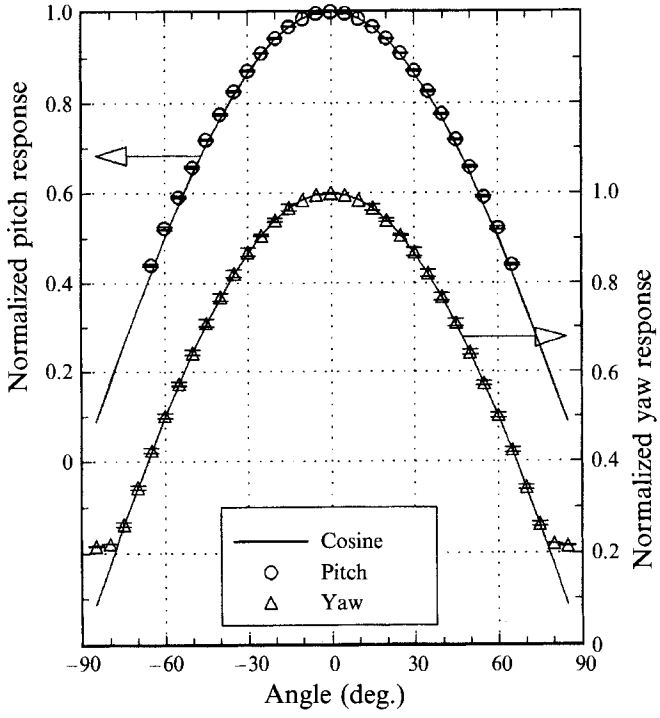

FIGURE 10. DAV angle response normalized on velocity at zero pitch and yaw for a minimum peak correlation coefficient of 0.95, $\omega_c^* = 5.65$. Points show average over measurement volume, error bars show r.m.s. variation.

A computer program was written to generate one-component DAV signals for a range of conditions using the above expressions. The impulse response required in (16) was taken as that of a single-pole low-pass filter. The measurement process was then simulated by applying the cross-correlation scheme. A seven point least-squares parabola was then used to interpolate the time delay of the cross-correlation peak. Velocity inferred from this transit time was then compared to the velocity input to the calculation for a range of conditions.

We begin by presenting calculations for the present DAV for which

$$D/\sigma = 1.04,\ h/D = 4.39,\ d/D = 0.019,\ \sigma = 0.1 \text{ mm}$$

and $\omega_c = 2\pi \times 140000\ \text{s}^{-1}$. Figure 8 illustrates the response to a uniform flow at zero yaw and pitch ($\alpha = 0, \beta = 0$). For this special case the response is not a function of y_0 at z_0. Computed over actual velocity, u_{DAV}/q, is plotted as a function of ω_c^*, which varies inversely with the absolute flow speed. The DAV appears closely linear, u_{DAV}/q varying from 1.024 at $\omega_c^* = 0.5$ (176 m s^{-1}) to 1.006 at $\omega_c^* = 50$ (1.76 m s^{-1}). For most applications this variation would be insignificant and so the error in u_{DAV} can be accounted for simply by multiplying by a constant factor.

Figure 9 shows the response of the DAV in pure pitch ($\beta = 90°$) and in pure yaw ($\beta = 0$) for $\omega_c^* = 5.65$ (15.6 m s^{-1}). Since the pitch and yaw characteristics will in general be functions of y_0 and z_0, respectively, the mean response (indicated by the points) and its r.m.s. variation over the measurement volume (shown by the error bars) are presented. For these averages the y- and z-limits of the measurement volume were

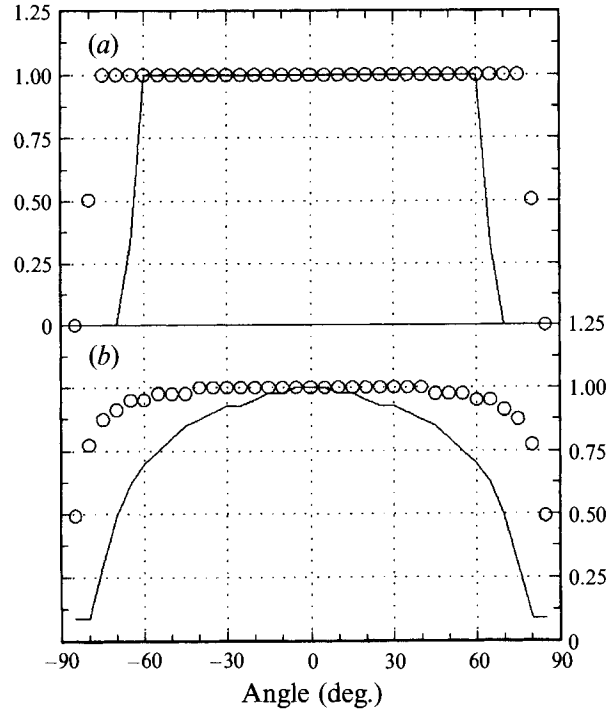

FIGURE 11. Proportion of measurment volume sensitive to a particular flow angle, $\omega_c^* = 5.65$: (*a*) pitch, (*b*) yaw. Lines are for current photodiode array with a minimum peak correlation coefficient of 0.95. Points are for improved photodiode-array design with a minimum peak correlation coefficient of 0.9.

taken to be $\pm 2\sigma$ (i.e. the $1/e^2$ points) and $\pm \frac{1}{2}h$ respectively. Between about $\pm 65°$ the pitch response appears good; the mean is closely cosinusoidal and the r.m.s. variations are small. The yaw response, however, is unacceptable even at small angles, the mean errors and r.m.s. variations being far too large. The reason for the poor performance is that at large yaw angles or z_0, many particle images cross the ends of the photodiode elements rather than their long edges.

To improve the response without changing the photodiode array geometry, signals produced by images crossing the photodiode ends need to be identified and ignored. A fairly good identifier is the magnitude of the peak cross-correlation coefficient. This is close to unity for images crossing the long edges of the diode elements but much smaller for most of those crossing the ends. Figure 10 shows pitch and yaw characteristics when signals with a peak correlation coefficient of less than 0.95 are ignored. The yaw response is greatly improved, the mean being cosinusoidal up to $\pm 75°$ and the r.m.s. remaining acceptably small. For angles less than about 65° the pitch response appears unaltered. For greater angles it is eliminated, however, indicating some bias against higher flow angles. This is shown more clearly in figure 11 where the proportion of the measurement volume sensitive to a particular flow angle is plotted *vs.* flow angle. For the pitch response this remains unity over almost the entire angle range. For yaw, it drops more gradually with increase in angle, but most of the loss still comes at angles greater than 60°. Although the results of figures 10 and 11 were calculated for $\omega_c^* = 5.65$ they are not a strong function of this parameter. Calculations with ω_c^* values between 1.4 and 45.2 show very similar results, the only significant effect being a slight reduction in the pitch response limit with ω_c^*.

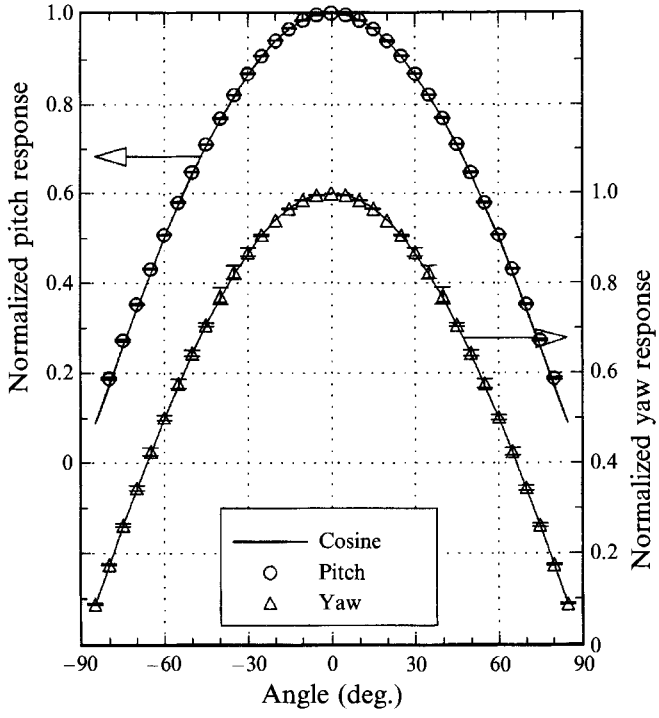

FIGURE 12. DAV angle response normalized on velocity at zero pitch and yaw for improved photodiode-array design. $\omega_c^* = 5.65$, minimum peak correlation coefficient = 0.9. Points show average over measurement volume, error bars show r.m.s. variation.

While the angle response of the present DAV may not be ideal it is important to remember that it has been achieved using a photodiode array not actually designed for the present purpose. Even if the design is restricted to two rectangular elements, the response can be substantially improved by increasing the aspect ratio of the array, h/D, and reducing the ratio of measurement volume to beam size, D/σ. For example, figure 12 shows the angle response for $h/D = 17.6$, $D/\sigma = 0.52$ and $d/D = 0.02$ with a minimum peak correlation coefficient of 0.9. The mean pitch and yaw response are nearly perfect cosines to 80 and 85° respectively while r.m.s. variations remain small. The angle bias (figure 11) and nonlinearity (figure 8) are also substantially reduced. Note that some increase in effective aspect ratio could be achieved by tilting the present photodiode array about its long axis, decreasing its width as viewed from the receiving lens. There are limits to this measure, however. For tilt angles much greater than 45°, particle images become obscured by the array casing and reflection of light from the photodiodes or their glass cover becomes a problem.

4. Measurements

Measurements were made in attached and separated turbulent flows to examine the performance of the one-component DAV experimentally. Where possible comparisons were made with a hot-wire anemometer. The flows were generated in a small blow-down open-circuit wind tunnel (see Smith, Rife & Devenport 1990). The tunnel has a rectangular test section 2.29 m long and 0.235 m wide. The last 0.330 m of its length, where the measurements were made, is built from Plexiglas (figures 2 and 13). The

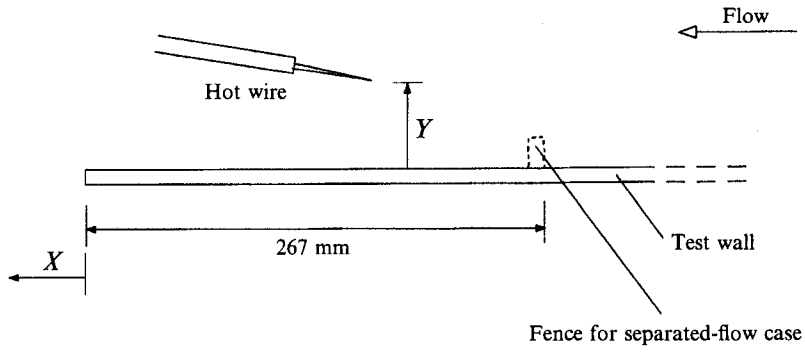

FIGURE 13. Schematic of the wind-tunnel test section viewed in the Z-direction. Note: hot-wire sensor parallel to wall and normal to mean flow.

height of the test section increases gradually along its length to maintain a zero streamwise pressure gradient, and is about 114 mm in the measurement section. Here the wind-tunnel wall boundary layers dominate the flow, having almost entirely engulfed the potential core. Measurements were made in the flow adjacent to the side test wall, shown in figure 2, along horizontal (Y) profiles at the mid-height of the test section. Figures 2 and 13 show the coordinate system to be used in presenting results. Note that X is measured downstream from the wind tunnel exit and is thus always negative. A Pitot-static probe, located at $X = -343$ mm, was used to monitor velocity in the potential core during measurements.

Hot-wire measurements were made using a TSI type 1210 T1.5 single sensor probe (figure 13) positioned using a computer-controlled traverse gear. The probe was operated using a Dantec 56C17/56C01 anemometer system (balanced for a frequency response of better than 30 kHz) connected through an Analogic HS-DAS 12 A/D converter to an IBM AT computer. The hot wire was calibrated in the potential core against the reference Pitot static. Temperature variations during calibration and measurement, at most ± 2 °F, were corrected using the method of Bearman (1971). The absolute position of the sensor was found by placing it as close as possible to the test wall and then using a cathetometer to measure the distance between the hot-wire prongs and their reflection in the wall, the overall accuracy being better than ± 0.1 mm. For the attached flows this uncertainty was further reduced by comparison of the mean-velocity measurements with a theoretical sublayer profile. This comparison led to a Y-datum adjustment of -0.06 mm in both flows, an error attributed to backlash in the traverse gear.

For measurements with the DAV, 2.1 μm polylatex spheres were introduced to the flow through a jet-type atomizer (Seegmiller 1985) placed at the blower outlet. The spheres were suspended in alcohol which evaporated soon after their injection into the flow, resulting in a monodisperse distribution of particle sizes. To enable DAV measurements close to the test wall the laser beam was introduced at a slight angle (0.6°) to the Z-axis (see figure 2). Its diameter in the measurement volume, estimated by measuring the beam diameter and convergence angle at the collimator output and the optical path length, was adjusted to 0.4 mm at the $1/e^2$ points. Judging from the shapes of the DAV signals, a smoother, more Gaussian intensity distribution was achieved if the beam was brought to its focus before, rather than after, the measurement volume. A dial indicator mounted between the outside of the test wall and optical table was used to indicate the relative Y-location of the DAV measurement volume, to a precision of ± 0.02 mm. The Y-location of the wall was determined to an

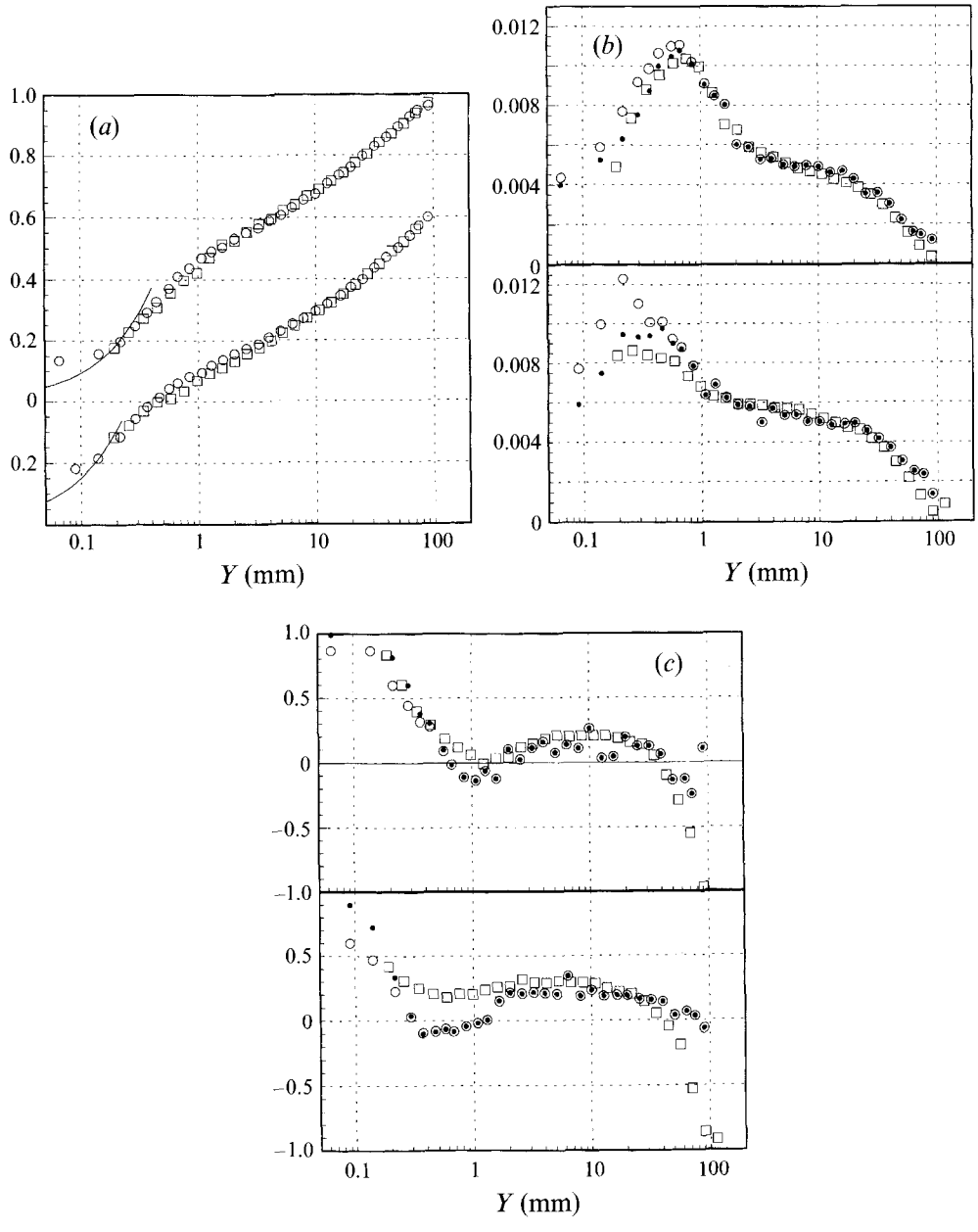

FIGURE 14. Profiles in the attached flows, upper curves, $U_e = 10$ m s^{-1}; lower curves, $U_e = 20$ m s^{-1}. (*a*) U/U_e; ○, DAV; □, hot-wire; ——, theoretical sublayer profile (friction velocity determined from slope of semi-log region). (*b*) $\overline{u'^2}/U_e^2$ and (*c*) U-skewness: ○, DAV; □, hot-wire; ●, DAV corrected for velocity-gradient broadening.

accuracy of better than ± 0.1 mm by maximizing the d.c. outputs of the photodiode amplifiers; with the measurement-volume centre at the wall, light power scattered by the wall and received by the photodiode array should be at a maximum. For the attached flows the Y-uncertainty was further reduced by comparison of the mean-velocity measurements with a theoretical sublayer profile. This comparison led to a Y-datum adjustment of $+0.04$ mm in both flows, the consistency of this error suggesting some bias in the above scheme. Note that, in contrast to LDA, scattered light from the

	Hot wire	DAV
U_l/U_e	0.01	0.004
$\overline{u'^2}/U_e^2$	0.0004	0.0004
U-skewness	0.07	0.17

TABLE 1. Typical uncertainty intervals. The uncertainty in DAV is from a limited number of samples and U_e normalization only.

wall is not a problem in making near-wall measurements since it merely adds a d.c. level to the signals.

At most measurement locations typically 400 measurable signals per second were visible in the DAV outputs, this rate being consistent with seeding density and measurement volume dimensions. Signals were cross-correlated by reading them into an IBM AT computer using a Rapid Systems R2000 A/D converter, the A/D inputs being buffered with two $\times 10$ buck and gain amplifiers. The R2000 is an 2-channel 8-bit A/D converter. Its external trigger was used to detect the presence of a signal by monitoring one of the DAV outputs. Since pre-trigger samples were taken, the same output could be used regardless of flow direction. The trigger level was set just above the noise level. At most locations, 192 pre- and 320 post-trigger samples were taken simultaneously on both channels, the sampling rate being adjusted between 20 Mhz and 500 kHz according to local flow conditions. Cross-correlations were performed with the aid of an 18-8 Laboratories PL2500 array processor. As in the simulation a seven-point least-squares parabola was used to interpolate the position of the peak. To allow further study of the DAV characteristics, signals were also stored on optical disc (a procedure that would not normally be necessary). Writing to disc was a relatively slow process and reduced the data rate to about 15 per second. Between 1000 and 4000 DAV signals were processed at each measurement point. Statistics were calculated using particle averages.

4.1. *Attached flows*

Measurements were made in the undisturbed test-wall boundary layer at $x = -165$ mm for edge velocities for 10 and 20 m s^{-1}. Figure 14 compares hot-wire and DAV measurements of mean velocity U/U_e, normal turbulence stress $\overline{u'^2}/U_e^2$ and skewness factor $\overline{u'^3}/(\overline{u'^2})^{1.5}$. Typical uncertainties are listed in table 1. Uncertainties for the DAV only include contributions from the limited number of velocity samples and the normalization on U_e, since the purpose of the measurements was to observe all other errors.

Agreement between the mean velocity measurements (figure 14*a*) appears very good. The largest difference, 2.5% U_e at 10 m s^{-1} and 3.5% U_e at 20 m s^{-1}, occur in the buffer layer where the hot-wire measurements lie slightly below those of the DAV. The DAV appears capable of useful velocity measurements as close as 0.2 mm from the wall, within the sublayer at 10 m s^{-1}. This limit is consistent with the 0.4 mm depth of the measurement volume.

Agreement between the turbulence stress measurements (figure 14*b*) is also satisfactory except in the near-wall region ($y < 0.8$ mm) and close to the outer edge of the boundary layer ($y > 40$ mm). The discrepancies in the near-wall region are almost certainly caused by velocity-gradient broadening of the DAV measurement, i.e. an additional apparent turbulence stress due to variations in mean velocity across the measurement volume. This error is well documented for LDA applications (see for example Durst, Melling & Whitelaw 1981). To first order the additional turbulence

stress is given by $(\Delta\partial U/\partial Y)^2$, where Δ is a distance representing the standard deviation of the distribution with Y of particles passing through the measurement volume. We would expect this distance to be at most 0.1 mm for the DAV. In fact, setting $\Delta = 0.065$ mm corrects well for the differences between the hot-wire and DAV results, especially at 10 m s^{-1}. The differences in the normal-stress measurements in the outer region are primarily due to electrical noise in the DAV. Consistent with equation (4) this error is not constant across the boundary layer but decreases rapidly with the mean velocity as the wall is approached. In both flows it adds about $0.001U_e^2$ to the normal stress at the furthermost point from the wall ($Y = 91$ mm). That this error is almost the same at 10 and 20 m s^{-1} is at odds with (4) unless a change in $\overline{t_n'^2}$ is allowed. Such a change is likely since this parameter was found to be quite sensitive to the optical alignment, which was adjusted between profiles. A second, but in this case insignificant, contributor to this error is broadening caused by the variation in particle image magnification with Y through the measurement volume. It is simple to show that the additional turbulence stress from this source is given by $(f\Delta(f_1-f)^{-2}M^{-1}U)^2$ where f is the focal length of the receiving lens, f_1 its distance from the measurement volume and Δ is defined above. This gives $4.2\times10^{-5}U^2$ for the present system. Note that the lower limit on normal stress measurements observed in these measurements is not fundamental and could be decreased by increasing laser power and/or adjusting the optical arrangement.

As with the normal stress, agreement between the measurements of skewness factor (figure 14*c*) is best in the mid region of the boundary layer. Close to the wall ($Y < 1.5$ mm) the DAV consistently underestimates skewness by about 0.2, slightly greater than the purely statistical uncertainty. In the very near-wall region ($Y < 0.5$ mm) this appears to be due to velocity-gradient broadening of the normal stress, since here correcting the normal stress using $\Delta = 0.065$ mm brings the two measurements into closer agreement. The remaining discrepancy may be partly due to second-order broadening, i.e. curvature of the mean profile within the volume. This error, which would tend to make the skewness more negative, would be greatest in the buffer layer, much like the differences observed here.

It is worth noting that the streamwise distance over which particle velocities are measured with the one-component DAV is only 5×10^{-5} m, considerably smaller than the corresponding dimension of most LDA measurement volumes. Transit times are correspondingly small and, in the above flows, of the same magnitude as the probable Kolmogorov timescale. Thus, with a sufficient data rate (achieved by increasing seeding density) meaningful velocity spectra could presumably have been measured. In flows of higher velocity, the Kolmogorov timescale τ would be smaller, but so would the transit time T, the ratio of T/τ varying as $U^{\frac{1}{2}}$. If necessary, measurement-volume size could be reduced to offset this by further focusing the laser beam and increasing the magnification of the receiving lens.

4.2. *Separated flow*

The satisfactory performance of the DAV in the attached flows, while gratifying, could have been predicted from its theoretical angle response curves. At the relatively small instantaneous flow angles experienced in a turbulent boundary layer these are closely cosinusoidal. In a separated flow, however, instantaneous flow angles reach 90° and some errors would be expected. Observing these errors was only one reason for performing separated-flow measurements. The primary purpose was to uncover any other unforeseen problems that would limit the performance of DAVs with better photodiode-array designs.

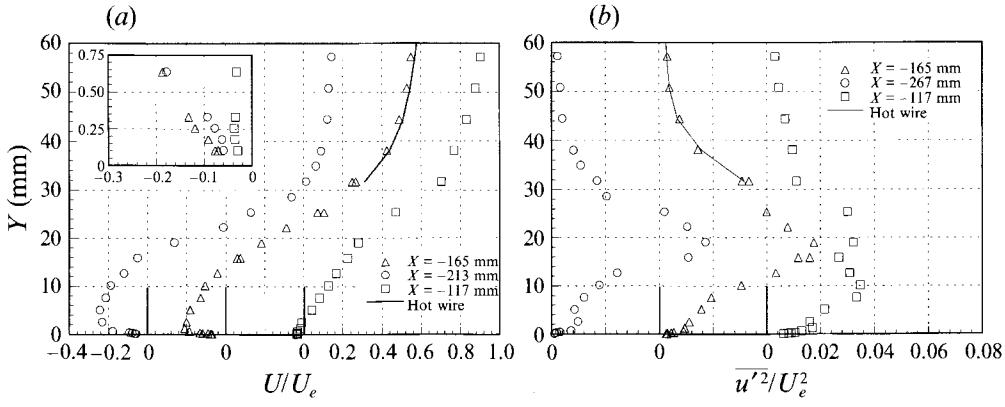

FIGURE 15. (a) U/U_e and (b) $\overline{u'^2}/U_e^2$ profiles in the separated flow. Inset shows detail of near-wall region.

A separated flow was generated by placing a fence on the test wall at $X = -267$ mm, figure 13. The fence had a rectangular cross-section 12.7 by 6.4 mm and completely spanned the test wall. It generated a region of recirculating flow roughly 150 mm in length. The DAV was used to measure profiles at $X = -117$, -165 and -213 mm for an approach edge velocity U_e of 10 m s^{-1}. Hot-wire measurements were made only at $X = -165$ mm, outside of the separation region where local turbulence levels were less than 30%. Because of the high turbulence intensities and instantaneous flow reversals in this flow the particle averaging used to determine statistics from the DAV measurements was expected to produce some bias error. This type of error has been well researched for LDA applications (see for example Fuchs *et al.* 1992) and was corrected, as it usually is for LDA, by weighting each velocity sample by the measurement-volume transit time of the particle that produced it.

Figure 15 shows mean velocity and normal turbulence stress profiles. Broadly speaking these measurements are consistent with the results of previous recirculating-flow studies (see for example Eaton & Johnston 1980; Adams, Johnston & Eaton 1984; Devenport & Sutton 1993). Qualitatively, at least, they demonstrate the ability of the DAV to make useful measurements in a reversing flow.

The mean profiles (figure 15*a*) show the steep velocity gradient associated with the separated shear layer and its relaxation with distance downstream. They also show the mean backflow which has a peak magnitude of $-0.24U_e$ at $X = -213$ mm (4.27 fence heights H from separation) and $-0.21U_e$ at $X = -165$ mm (8.06H from separation). The profile at $X = -117$ mm appears to be measured close to the reattachment location. Also visible at $X = -165$ and -213 mm are the 'sub-boundary layers' formed underneath the backflow. A close examination of the near-wall sections of these profiles (inset to figure 15*a*) shows them to be consistent with the no-slip condition down to about 0.2 mm from the wall. This lower limit on Y is in agreement with the attached-flow results. The profiles of normal turbulence stress (figure 15*b*) also show the separated shear layer. At $X = -213$ and -165 mm the peak turbulence normal stress is $0.057U_e^2$ (23.9% turbulence intensity). By $X = -117$ mm it has dropped to $0.035U_e^2$ (18.7%). Agreement with the hot-wire measurements made in the outer part of the shear layer at $X = -165$ mm appears satisfactory.

Without quantitative comparisons the limitations of the DAV angle response are not visible in the above measurements. They are visible, however, in velocity histograms. Figure 16 shows a selection of histograms from the profile at $X = -165$ mm. At all

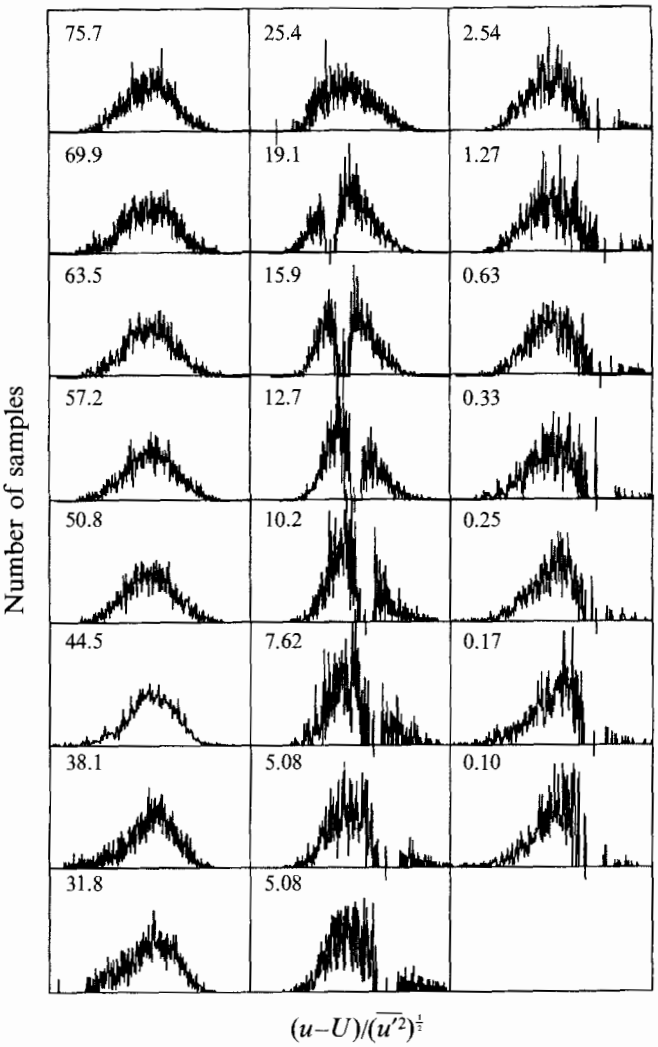

FIGURE 16. Velocity histograms measured in the separated flow at $X = -165$ mm. The number in the top left-hand corner of each histogram indicates the y-location in mm. Tick on horizontal axes indicates location of zero velocity.

locations where instantaneous flow reversals occurs the histograms have a 'hole' in the vicinity of zero velocity. While this is almost certainly a consequence of the imperfect angle response it is also due to the limited duration of the signals recorded by the A/D converter with each particle transit. The finite record duration limits the maximum measurable transit time and thus the minimum velocity magnitude. The effects of increasing the duration can be seen by comparing the histograms measured at $Y = 10.2$ and 7.6 mm, for example, and noting the difference in $\overline{u'^2}/U_e^2$ at these locations (figure 15*b*). Between these points the duration was doubled by halving the sampling rate, resulting in a corresponding reduction in the size of the hole. In general, however, reducing the sampling rate may not be the best way of controlling this phenomenon since it degrades the resolution of the DAV for small transit times (i.e. high velocities), forcing a heavy reliance on the scheme used to interpolate the cross-correlation function. In most separated flows, as in this one, there are points where both high

velocities and near-zero velocities occur. A more satisfactory solution is to increase the record duration by increasing the number of samples. An alternative would be count the number of records for which signals are detected on one channel but not the other and then assign these samples a velocity of zero. This type of scheme has been successfully implemented with pulsed-wire anemometers (Bradbury & Castro 1971).

In summary, the separated flow measurements revealed no fundamental problems that could limit the accuracy of improved DAV designs.

5. Conclusions and future work

An optical technique for measuring turbulent flows has been proposed. Diode-array velocimetry involves timing the passage of seed particles through a small section of a light beam by timing the passage of their images across one or more photodiode arrays. The shapes and positions of the array elements are chosen to make the deduction of flow properties from the measured transit times simple and accurate.

A DAV for one-component velocity measurements has been developed to demonstrate this concept. This device uses a single photodiode array with two long rectangular elements placed side by side (figure 3). A 0.4 mm diameter laser beam is used to illuminate seed particles in a fluid flow. Light scattered by the particles at 90° to the beam is collected by a lens and focused onto the array, resulting in a measurement volume consisting of two parallel 'plates' $0.104 \times 0.457 \times 0.4$ mm (figure 4). The transit time of particles between the plates and thus the velocity component normal to them was measured by cross-correlating the amplified electrical outputs of the photodiode elements.

The sensitivity of this DAV to electrical noise has been examined theoretically. Noise produces an apparent additional normal turbulence stress, the magnitude of which decreases as the size of the measurement volume is reduced. The DAV angle response has been examined by simulating the signals generated by the photodiode elements for a range of conditions. Yaw and pitch response are closely cosinusoidal to angles greater than 60° as long as signals producing peak correlation coefficients less than 0.95 are ignored. These limitations are largely a function of photodiode design. Even if the design is restricted to two rectangular elements, the response can be substantially improved by lengthening the elements and reducing their width relative to that of the beam.

Mean-velocity measurements made in two attached boundary-layer flows (edge velocity 10 and 20 m s^{-1}) agree well with hot-wire measurements. Normal-stress and skewness profiles are also in good agreement, except in the near-wall and edge regions. Improved agreement is obtained in the near-wall region after correcting for velocity-gradient broadening. Discrepancies in the edge region are a consequence of electrical noise which produced an apparent additional stress of about $0.001 U_e^2$. The DAV appears capable of mean velocity measurements down to about 0.2 mm from the wall.

DAV measurements made in the separated flow formed behind a fence (edge velocity 10 m s^{-1}) show all expected features of the separated shear layer and recirculation including the sub-boundary layer formed beneath the backflow. Histograms measured in the reversing part of this flow show a hole near zero velocity that is consequence of the imperfections in the DAV angle response and the limited duration of the photodiode signals correlated to determine the transit time. Neither of these problems is fundamental. Using a better photodiode-array design and increasing the duration of the photodiode signals used in the cross-correlation should eliminate or, at least, greatly reduce this effect.

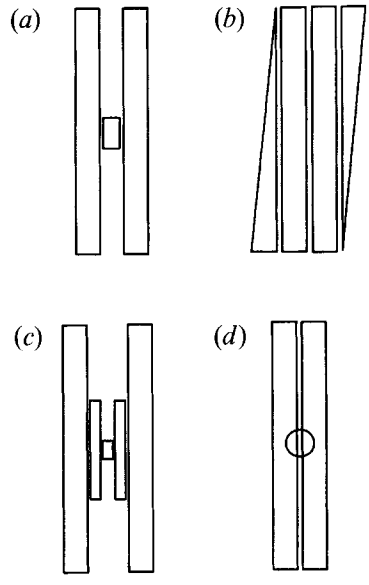

FIGURE 17. Some proposed photodiode array designs. (*a*) For improved accuracy in one-component velocity measurements, (*b*) for one-component velocity and position measurements, (*c*) for multiple velocity measurements on the same particle, (*d*) for improved accuracy in one-component measurements (circular element is optically overlayed on rectangular elements).

There are a number of future possibilities for development of the DAV. Perhaps the most pressing is construction of an improved photodiode array for one-component velocity measurements. Figure 17(*a*) is a possible design consisting of a two long thin rectangular elements with a shorter element sandwiched between them. Velocity component is measured using the long elements. The short element is used to distinguish particle images that cross the central portion of the array from those that do not. Eliminating the latter would greatly improve pitch response and substantially decrease measurement-volume size. Furthermore this design works well with the trigger timing scheme (Devenport & Smith 1993). Successful implementation of the trigger timing scheme would allow photodiode array and signal processing to be integrated into a simple package. Apart from making the DAV cheaper and easier to use it would be practicable to operate many such packages in parallel, making simultaneous velocity measurements over a line or grid of points possible.

Further in the future we anticipate a range of photodiode arrays designed for different purposes and the use of more than one array and/or receiving angle for two- or three-component measurements. Figure 17(*b*) shows a one-component velocity and position sensing array – the inner two elements are used to sense velocity, the outer two the location of the particle image. Accuracy of velocity measurements could be improved by making a sequence of two or more measurements on the same particle, as implied by the design in figure 16(*c*). Such a device, at least in principle, could also measure particle acceleration. A potentially useful technique in DAV design is to optically overlay different photodiode arrays by splitting light focused by the receiving lens and examining the same part of the image with different detectors. This technique could be used to overlay a small circular element at the centre of the present photodiode array (figure 17*d*), for example, the combination being used in much the same way as the array of figure 17(*a*). Avalanche photodiodes (APDs) may be well suited to some of these designs. Depending on circumstances, APDs produce less noise

and have a much better frequency response so, given equation (10), could significantly improve DAV performance.

The authors gratefully acknowledge the support of the National Science Foundation under award 9011071, the Office of Naval Research, under grant number N00014-92-J-1292 and their program managers, Dr Stephen C. Traugott and Mr James A. Fien. We would also like to thank Mr Ken Wittmer and Mr Michael Rife for their assistance with the hot-wire measurements and Dr Roger Simpson for his helpful advice.

Appendix. Dependence of t'_n

If transit time is determined from the DAV output signals using a trigger scheme one would expect the r.m.s. of t'_n to vary approximately as the r.m.s. electrical noise level divided by the rate of change of voltage at the leading edge of the signal where the trigger is fired, i.e.

$$(\overline{t'^2_n})^{\frac{1}{2}} \sim \frac{(\overline{v'^2_{noise}})^{\frac{1}{2}}}{\partial v/\partial t}. \tag{A 1}$$

Assuming that the time taken for the particle image to cross the edge of each photodiode element is negligible, the rate of change of voltage is determined approximately by the step response of the amplifier. It therefore depends on the peak signal magnitude V_s and the angular cutoff frequency ω_c,

$$\partial v/\partial t \sim V_s \omega_c \tag{A 2}$$

and so

$$\frac{(\overline{t'^2_n})^{\frac{1}{2}}}{T} \sim \frac{1}{S\omega_c T} \tag{A 3}$$

where $S = V_s/(\overline{v'^2_{noise}})^{\frac{1}{2}}$.

Now consider the situation where the transit time is determined as the time delay of the peak cross-correlation $R_{xy}(\tau) = \overline{x(t)\,y(t+\tau)}$. Here x and y are used to denote the two DAV signals. Determining the peak in R_{xy} is the same as determining the zero-crossing point of its first derivative. $(\overline{t'^2_n})^{\frac{1}{2}}$ will thus vary as the uncertainty due to noise in $\partial R_{xy}/\partial\tau$ divided by $\partial^2 R_{xy}/\partial\tau^2$. Now,

$$\frac{\partial R_{xy}}{\partial\tau} = \overline{x(t)\frac{\partial y(t+\tau)}{\partial\tau}} = \overline{x_s(t)\frac{\partial y_s(t+\tau)}{\partial\tau}} + \overline{x_n(t)\frac{\partial y_s(t+\tau)}{\partial\tau}} + \overline{x_s(t)\frac{\partial y_n(t+\tau)}{\partial\tau}} + \overline{x_n(t)\frac{\partial y_n(t+\tau)}{\partial\tau}}, \tag{A 4}$$

where x_s and x_n, and y_s and y_n are used to denote the signal and noise components of x and y respectively. The last three terms of (A 4) express the uncertainty due to noise in $\partial R_{xy}/\partial\tau$. They are non-zero because only finite lengths of x and y are correlated. One would expect the third of these to be negligible for significant signal-to-noise ratios. The other two should scale as $(\overline{v'^2_{noise}})^{\frac{1}{2}} V_s \omega_c$ since the electrical noise is governed by the same amplifier-frequency response as the signal. The second derivative of the correlation is

$$\frac{\partial^2 R_{xy}}{\partial\tau^2} = \overline{x(t)\frac{\partial^2 y(t+\tau)}{\partial\tau^2}}, \tag{A 5}$$

which should scale as $V_s^2\omega_c^2$. Dividing these two results we once more obtain (A 3).

REFERENCES

ADAMS, E. W., JOHNSTON, J. P. & EATON, J. K. 1984 Experiments on the structure of a turbulent reattaching flow. *Rep.* MD-43. Dept. of Mech. Engng, Stanford University.

BEARMAN, P. W. 1971 Corrections for the effect of ambient temperature drift on hot-wire measurements in incompressible flow. *DISA Information*, vol. 11, pp. 25–30.

BRADBURY, L. J. S. & CASTRO, I. P. 1971 A pulsed-wire technique for velocity measurements in highly turbulent flows. *J. Fluid Mech.* **49**, 657–691.

BOUTIER, A. & LEFEVRE, J. 1988 Mosaic laser velocimeter. In *4th Symp. on Applications of Laser Anemometry to Fluid Mechanics, Lisbon, Portugal.*

DEVENPORT, W. J. & SMITH, E. J. 1993 Development of the one component diode array velocimeter. *Rep.* VPI-AOE-201. AOE Dept., VPI & SU.

DEVENPORT, W. J. & SUTTON, E. P. 1993 An experimental study of two flows through an axisymmetric sudden expansion. *Exp Fluids* **14**, 423–432.

DURST, F., MELLING, A. & WHITELAW, J. H. 1981 *Principles and Practice of Laser Doppler Anemometry*. Academic.

EATON, J. K. & JOHNSTON, J. P. 1980 Turbulent flow reattachment: an experimental study of the flow and structure behind a backward-facing step. *Rep.* MD-39. Dept. of Mech. Engng, Stanford University.

FUCHS, W., ALBRECHT, H., NOBACH, H., TROPEA, C. & GRAHAM, L. J. W. 1992 Simulation and experimental verification of statistical bias in laser Doppler anemometry including non-homogeneous particle density. In *6th Symp. on Applications of Laser Anemometry to Fluid Mechanics, Lisbon, Portugal.*

HIRLEMAN, E. D., YUE, Y., BERMAN, N. S. & GUAN, D. X. 1984 Single laser beam velocimetry (L1V) in turbulent flows. In *2nd Symp. on Applications of Laser Anemometry to Fluid Mechanics, Lisbon, Portugal.*

OHMURA, K., HISHADA, K. & MAEDA, M. 1992 A multi-angle laser-two-focus velocimeter using photodiode arrays. In *6th Symp. on Applications of Laser Anemometry to Fluid Mechanics, Lisbon, Portugal.*

SEEGMILLER, H. L. 1985 Seeding subsonic, transonic and supersonic flows with 0.5 μm polystyrene latex spheres. In *Wind Tunnel Seeding Systems of Laser Velocimeters, NASA* CP-2393.

SMITH, E. J., RIFE, M. C. & DEVENPORT, W. J. 1990 Investigations of the small boundary-layer tunnel. *Rep.* VPI-AOE-177. AOE Dept., VPI & SU.